
This is an electronic reprint of the original article.
This reprint may differ from the original in pagination and typographic detail.

Stene, Riane E.; Scheibe, Benjamin; Pietzonka, Clemens; Karttunen, Antti J.; Petry, Winfried; Kraus, Florian

MoF₅ revisited. A comprehensive study of MoF₅

Published in:
Journal of Fluorine Chemistry

DOI:
[10.1016/j.jfluchem.2018.05.002](https://doi.org/10.1016/j.jfluchem.2018.05.002)

Published: 01/07/2018

Document Version
Peer-reviewed accepted author manuscript, also known as Final accepted manuscript or Post-print

Published under the following license:
CC BY-NC-ND

Please cite the original version:
Stene, R. E., Scheibe, B., Pietzonka, C., Karttunen, A. J., Petry, W., & Kraus, F. (2018). MoF₅ revisited. A comprehensive study of MoF₅. *Journal of Fluorine Chemistry*, 211, 171-179.
<https://doi.org/10.1016/j.jfluchem.2018.05.002>

This material is protected by copyright and other intellectual property rights, and duplication or sale of all or part of any of the repository collections is not permitted, except that material may be duplicated by you for your research use or educational purposes in electronic or print form. You must obtain permission for any other use. Electronic or print copies may not be offered, whether for sale or otherwise to anyone who is not an authorised user.

MoF₅ revisited. A comprehensive study of MoF₅.

Riane E. Stene ^{a,b}, Benjamin Scheibe ^a, Clemens Pietzonka ^a, Antti J. Karttunen ^c, Winfried Petry ^b and Florian Kraus ^{a,*}

Dedicated to Professor Erhard Kemnitz to further acknowledge his ACS Award for Creative Work in Fluorine Chemistry

^a Anorganische Chemie, Fachbereich Chemie, Phillips-Universität Marburg, Hans-Meerwein-Straße 4, 35032 Marburg, Germany

^b Department of Physics, Technische Universität München, Lichtenbergstraße 1 85748 Garching, Germany

^c Department of Chemistry and Material Science, Aalto University, 00076 Aalto, Finland

* Correspondence: florian.kraus@chemie.uni-marburg.de; Tel.: +49 6421 28 26668

Academic Editor: name

Received: date; Accepted: date; Published: date

Abstract: While the properties of molybdenum pentafluoride, MoF₅, have been investigated in the past, there exists no comprehensive study of the compound. Additionally, many of these studies appear incoherent and offer contradictory explanations of some of the observed properties of MoF₅. Consequently, a comprehensive examination of MoF₅ is presented here, including a redetermination of the crystal structure of MoF₅ using single crystal and powder X-ray diffraction, the reevaluation of its IR, Raman and UV-vis spectrum, and a study of its density (3.50(2) g/cm³ @ 25 °C) and magnetic properties. Additionally, density functional theory (DFT) calculations were performed on the gas phase molecule Mo₄F₂₀ to provide a discussion of properties realized during investigation. Single crystal X-ray diffraction showed MoF₅ to crystalize in the monoclinic, C2/m space group, as isolated tetramers having the formula Mo₄F₂₀. Magnetic measurements showed that when "MoF₅" is cooled from the melt fast enough, paramagnetic species with $S = \frac{1}{2}$ are present together with $S = 0$ species. These species may be described using the formula (MoF₅)_{*n*} (*n* = odd) and (MoF₅)_{*n*} (*n* = even, presumably *n* = 4). From the measurements, the content of the $S = \frac{1}{2}$ species is estimated to be 6 %. The preferred species of MoF₅ under ambient conditions is Mo₄F₂₀.

Keywords: crystal structure; IR spectroscopy; UV-vis spectroscopy; Raman spectroscopy; density; magnetic properties; molybdenum; fluoride; MoF₅ type; WOF₄ type

1. Introduction

The synthesis of molybdenum pentafluoride was first described by R. D. Peacock in 1957 as a result of passing dilute fluorine gas over molybdenum hexacarbonyl at -75 °C to produce Mo₂F₉, which decomposes at 170 °C under vacuum to give MoF₅ and MoF₄ [1]. However, due to the use of fluorine gas, this reaction was described by preceding authors as quite exothermic. Since, simpler techniques have been discovered to produce MoF₅, such as the method used in this work which was briefly described by Geichman and coworkers [2] and which will be elaborated upon here. In short, MoF₆ is reduced using carbon monoxide and ultraviolet radiation. After the volatile products are discarded, pure MoF₅ can be collected from the reaction vessel.

MoF₅ is a sunflower yellow powder which, at high purities, melts at 45.7 °C (318.9 K) [3] and reacts with moisture to give a blue hydrolysis product, likely belonging to the molybdenum blues class of compounds. However, other sources report the melting point of MoF₅ to be between 63 and 67 °C (336 – 340 K) [1,4,5] but our observations are in agreement with the lower reported melting point.

MoF₅ is reported to be soluble in anhydrous HF without decomposition [5], however, through this work it has been found that, while MoF₅ is stable in anhydrous HF, it has limited solubility in

the solvent at room temperature. It sublimes at 50 °C [5] and disproportionates at 165 °C, giving MoF₄ and MoF₆ [4], however, no atmospheric or pressure conditions were reported for these measurements. Interestingly, though, mass spectroscopic and electron-diffraction studies on overheated vapors of MoF₅ report the molecule to be stable at temperatures as high as 280 °C [6,7]. Additional properties of MoF₅ have been reported, albeit not a lot of work has been done on MoF₅ since the 1970's. UV-Vis [8], IR [9,10], and Raman data [9–11] are available for MoF₅, however, little to no explanation of the bands arising from these spectra is given in these works. The magnetic properties and electronic properties [12–14], vapor pressure curve [4], and other thermodynamic properties [3] of MoF₅ have also been studied.

Edwards and coworkers investigated the crystal structure of MoF₅ in 1962 [15]. However, they state "the intensities of the spots (collected from single crystal oscillation and Weissenberg photographs) were difficult to estimate" and that the observed differences of Mo1—F_{terminal} and Mo2—F_{terminal} bond lengths are "probably not significant". In our efforts to explore the chemistry of MoF₆ and MoF₅ in greater detail, we obtained single crystals of the latter and re-determined its crystal structure to a much higher accuracy. We also set out to describe the properties of the absorption spectra of MoF₅, and elaborate upon the magnetic measurements already described in the literature. Additionally, the density of MoF₅ was investigated and is reported here.

2. Results and Discussion

2.1 Single-crystal and powder X-ray structure analysis

MoF₅ crystallizes as fluorine-bridged tetramers having the formula Mo₄F₂₀ (M = 763.76 g/mol). Single crystal X-ray diffraction showed the crystal structure of MoF₅ as belonging to the monoclinic space group C2/m (no. 12). The lattice parameters of MoF₅ were calculated by LeBail refinement from a powder diffraction measurement taken at room temperature: $a = 9.6502(2)$, $b = 14.2451(2)$, $c = 5.3100(1)$ Å, $\beta = 93.088(1)^\circ$, $V = 728.89(2)$ Å³. These lattice parameters are in good agreement with those obtained by Edwards and coworkers ($a = 9.61(1)$, $b = 14.22(2)$, $c = 5.16(1)$ Å, $\beta = 94.21(20)^\circ$, $V = 703$ Å³) [15], however, no measurement temperature was reported for their data collection. The powder diffraction pattern of MoF₅ in Figure 1 shows the synthesized compound to be phase pure; the crystal parameters for MoF₅ are listed in Table 1.

MoF₅ crystallizes in the MoF₅ structure type (mS48, C2/m) which is sometimes referred to as the WOF₄ structure type [16] and is characterized by MoF₅-units forming tetramers having the Niggli formula $\infty^0[\text{MoF}_{2/2}\text{F}_{4/1}]$. The fluorine atoms in the crystal structure of MoF₅ pack in a distorted cubic closed packed array. An identical structural motif is observed in the compounds M₄F₂₀ (M = Nb, Ta), whereas the M₄F₂₀ structure found in the crystals of RuF₅, OsF₅, RhF₅ and PtF₅ (RuF₅ type, mP48, P2₁/c) is characterized by corrugated tetramers and fluorine atoms which pack in distorted hexagonal closed packed arrays. Moreover, the atomic distances and angles of MoF₅ are comparable to those of NbF₅ and TaF₅.

The crystal structure of MoF₅ can be seen in Figure 2 and the tetramer Mo₄F₂₀ motif formed by MoF₅ is presented in Figure 3. In the specific case of Mo₄F₂₀, there are two distinct types of Mo atoms, one residing on the Wyckoff position 4h (site symmetry 2; Mo1) and the other residing on 4i (site symmetry m; Mo2). In both cases, the Mo atoms experience octahedron-like coordination by six fluorine atoms, in which two of these fluorine atoms are bridging to other Mo atoms. The atomic distance between Mo1 to the μ -bridging fluorine atoms F4, which reside on the 8j (1) positions, are observed to be 2.0423(11) Å, whereas the Mo2— μ -F distance is 2.0463(11) Å. Both agree well within the 3 σ criterion. The μ -F—Mo—F_{trans} angles are essentially equal with a value of 178.04(6)° for Mo1 and 178.15(6)° for Mo2. Edwards and coworkers reported a Mo1—F4 distance of 2.04(4) Å and a slightly longer Mo2—F4 distance of 2.09(4) Å [15], both of which agree with our findings. However, their reported μ -F—Mo1—F_{trans} and μ -F—Mo2—F_{trans} angles are both 180.0(2)°.

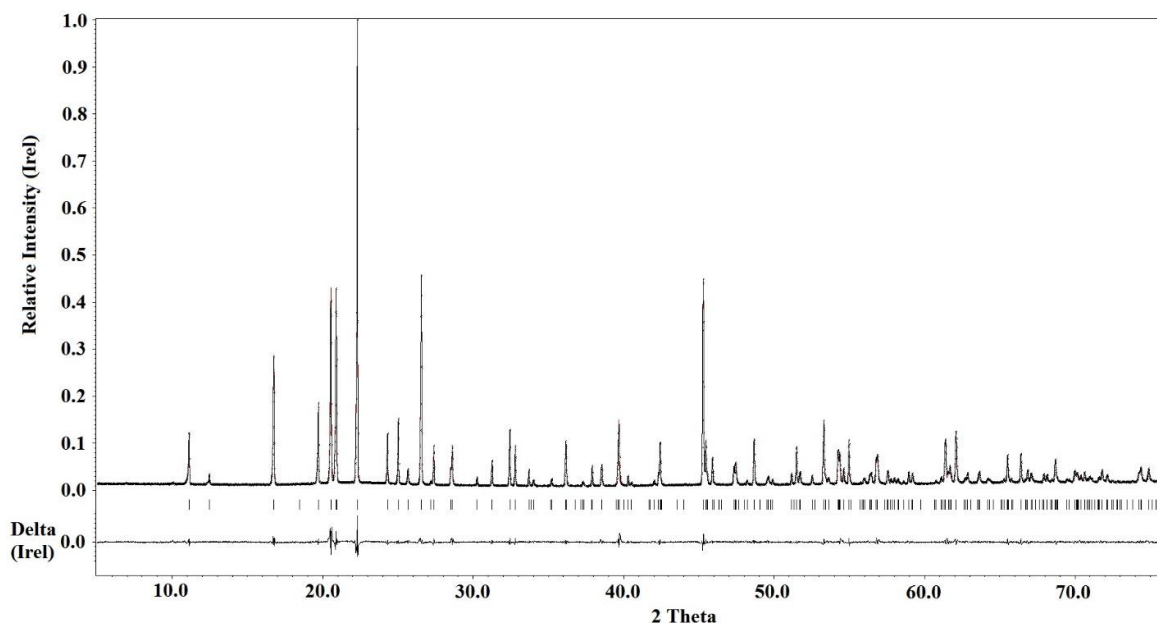


Figure 1. Powder diffraction pattern of MoF₅ measured at 293 K, processed through the Jana2006 program using a Le Bail refinement. The observed powder diffraction pattern is shown in black, while the calculated powder diffraction pattern is shown in red (barely visible due to good agreement). The difference between the observed and calculated patterns is shown by the black difference curve at the bottom of the schematic.

The atomic distances of Mo1—F5, Mo2—F1 and Mo2—F2, which are the distances to the so called axial F-atoms, are 1.8012(13), 1.8013(18) and 1.8011(18) Å, respectively, and are thus essentially identical. The distances of Mo1—F6 and Mo2—F3, where the respective F atoms are in trans position to the μ -F atoms and thus will be called equatorial F atoms, are slightly elongated with distances of 1.8236(14) and 1.8183(13) Å, respectively. Thus, the equatorial F atoms exhibit larger distances to the Mo atoms by about 0.02 Å in comparison to the axial F atoms (F1, F2, and F5). It is interesting to note that this finding may be a representation of the structural trans effect [17,18]. However, to the best of our knowledge this has not been reported for (pseudo)octahedral, homoleptic complexes. In NbF₅ and TaF₅ the distances of the metal atoms to the terminal F atoms are very similar, or the same, if the 3σ criterion is applied and no clear difference in length of the equatorial or axial bonds is observed. Thus, this structural trans effect may arise from the d¹ electron configuration of the Mo atoms and will be elaborated upon in the Computational Results section.

Interestingly, the Mo1—F6 bond length reported by Edwards and coworkers (1.89(4) Å) [15], is rather unprecise than that reported here (1.8236(14) Å). It is unclear why Edwards and coworkers observed such an elongation for the equatorial F atoms on the Mo1 atom but this may be due to the problems they described for the estimation of spot intensities. In contrast to this elongation, their reported Mo2—F3 bond length is significantly shorter with a distance of 1.74(4) Å. For the axial F atoms (F5 on Mo1 and F1 and F2 on Mo2), atomic distances of 1.82(9), 1.66(1), and 1.69(1) Å were reported, respectively [15]. In our case, 1.8012(13), 1.8013(18) and 1.8011(18) Å are observed for these respective atomic distances.

As may be expected, the Mo—F atomic distances for the terminal F-atoms are smaller in comparison to those of the bridging fluorine atoms (2.0423(11) and 2.0463(11) Å) by about 0.22 Å for those in equatorial position and 0.24 Å for the axial ones.

Table 1. Crystallographic parameters for MoF₅. The middle column outlines parameters collected from single crystal X-ray diffraction (SCXRD) while the second column outlines parameters collected from powder X-ray diffraction (PXRD).

| | MoF ₅ (SCXRD) | MoF ₅ (PXRD) |
|---|---------------------------|-------------------------|
| empirical formula | MoF ₅ | MoF ₅ |
| color and appearance | transparent yellow cuboid | yellow powder |
| molecular mass [g/mol] | 190.94 | 190.94 |
| crystal system | Monoclinic | monoclinic |
| space group | <i>C2/m</i> (12) | <i>C2/m</i> (12) |
| <i>a</i> [Å] | 9.4719(7) | 9.6502(2) |
| <i>b</i> [Å] | 14.1200(7) | 14.2451(2) |
| <i>c</i> [Å] | 5.0856(4) | 5.3100(1) |
| β [°] | 96.191(6) | 93.088(1) |
| <i>V</i> [Å ³] | 676.20(8) | 728.89(2) |
| <i>Z</i> | 8 | 8 |
| ρ_{calc} [g cm ⁻³] | 3.751 @ 100 K | 3.4789 @ 293 K |
| ρ_{exp} [g cm ⁻³] @ 25 °C | — | 3.50(2) |
| λ [Å] | 0.71073 (MoK α) | 1.54051 (CuK α) |
| <i>T</i> [K] | 100 | 293 |
| μ [mm ⁻¹] | 3.854 (MoK α) | 30.368 (CuK α) |
| θ_{max} | 34.856 | — |
| 2 θ range measured (min, max, increment) | — | 5.007, 75.972, 0.015 |
| 2 θ range refined (min, max) | — | 5.007, 75.972 |
| <i>hkl</i> _{max} | -15 ≤ <i>h</i> ≤ 15 | — |
| Size [mm ³] | 0.13 × 0.12 × 0.17 | — |
| <i>R</i> _{int} , <i>R</i> _{σ} | 0.047 | — |
| <i>R</i> (<i>F</i>) (<i>I</i> ≥ 2 σ (<i>I</i>), all data) | 0.0264, 0.0287 | — |
| <i>wR</i> (<i>F</i> ²) (<i>I</i> ≥ 2 σ (<i>I</i>), all data) | 0.068, 0.0693 | — |
| <i>R</i> _{<i>p</i>} , <i>wR</i> _{<i>p</i>} | — | 0.0437, 0.0610 |
| <i>S</i> (all data) | 1.154 | — |
| data, parameter, restraints | 1511, 61, 0 | 4732, 23, 0 |
| $\Delta\rho_{\text{max}}$, $\Delta\rho_{\text{min}}$ [e Å ⁻³] | 1.08, -1.54 | — |

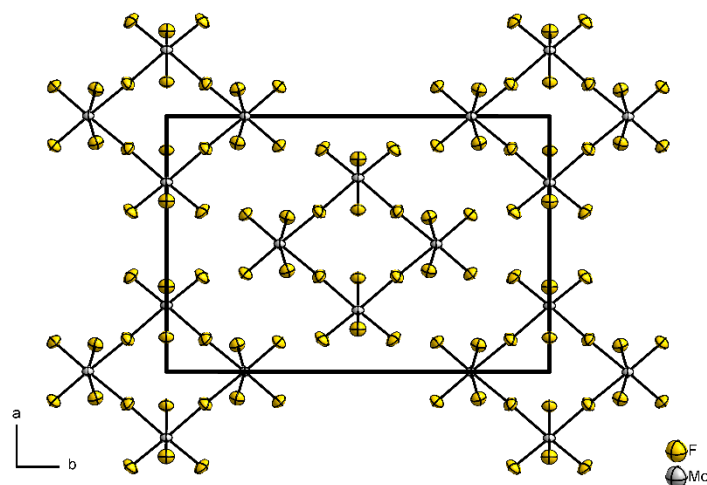


Figure 2. A section of the crystal structure of MoF₅ viewed along the *c*-axis. Displacement ellipsoids shown at the 70% probability level at 100 K.

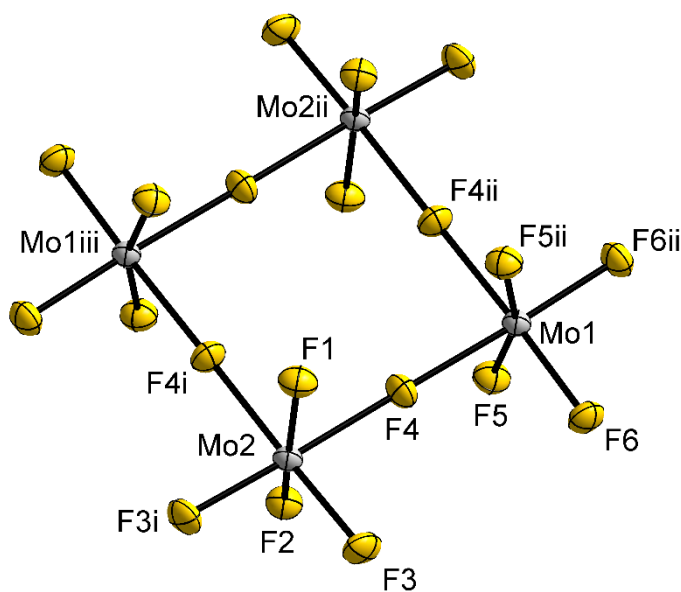


Figure 3. Structure of the MoF₅ tetramer unit displaying the MoF₄ units bridged through two fluorine atoms to two neighboring Mo atoms. Atom labeling in accordance to the manuscript by Edwards and coworkers [15]. Displacement ellipsoids are shown at the 70% probability level at 100 K. [Symmetry codes: (i) $x, -y, z$; (ii) $-x, y, 1 - z$; (iii) $-x, -y, 1 - z$.]

The point symmetry of the Mo₄F₂₀ molecule is $2/m, C_{2h}$, with the twofold rotation axis running through the Mo1 atoms and the perpendicular mirror plane bisecting the Mo2, F1 and F2 atoms. The Mo—Mo distance is 4.0881(3) Å, and the four membered ring formed by the Mo atoms is a flat square.

2.2. Electronic and Vibrational Spectroscopy

The electronic spectrum of MoF₅ dissolved in perfluoroether (C₈F₁₆O, FC-75, 3M) was studied in the range of 400 to 1100 nm (see Figure 4). The spectrum obtained was rather simple with absorption occurring in the near UV and blue regions (beginning at about 500 nm), and the

beginning of another absorption band starting at about 770 nm and extending into the near IR region of the spectrum. Peacock and Sleight studied the electronic spectrum of molten MoF₅ in the region of 4000 to 26000 cm⁻¹ (2500 to 385 nm) [8]. They observed a single band in the spectrum centered at 7500 cm⁻¹ (1333 nm). The single absorption band found in the work of Peacock and Sleight may arise from the same electronic transition giving rise to the absorption in the red and near IR regions in this work, however, a direct comparison cannot be made since both works obtained spectra using different sample conditions.

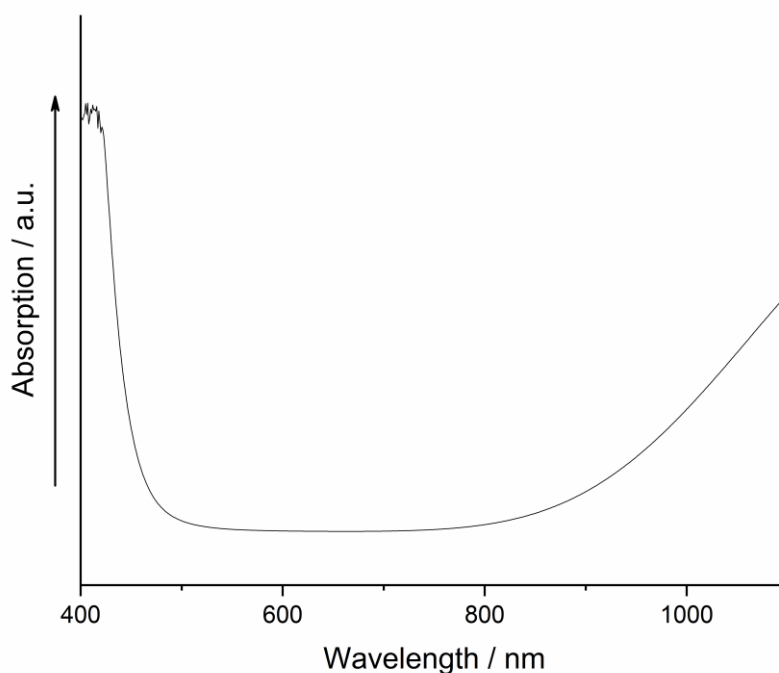


Figure 4. Visible and near IR spectrum of MoF₅ dissolved in perfluoroether.

IR spectroscopy was studied on a polycrystalline sample of MoF₅ at 25 °C in the region of 900 to 400 cm⁻¹. The IR spectrum obtained from this work shows five bands at approximately 762, 739, 720, 675 and 496 cm⁻¹. It can be said that the bands at 762, 739, 720 and 675 cm⁻¹ are all overlapping to some degree. Upon comparison of the measured IR spectrum to that of a IR spectrum calculated for the solid state of MoF₅ using the DFT-PBE0 method (a more detailed description of these calculations can be found in the Computational Results section), it can be seen that the peak positions correlate very well, however, the peak shapes and intensities vary. A comparison of the experimental and theoretical spectra is shown in Figure 5. Furthermore, peak assignments for the bands in the experimental IR spectrum were made utilizing the results of the theoretically calculated IR spectrum in which the theoretical vibrations were visualized using the Jmol software [19]. Band assignments are listed in Table 2.

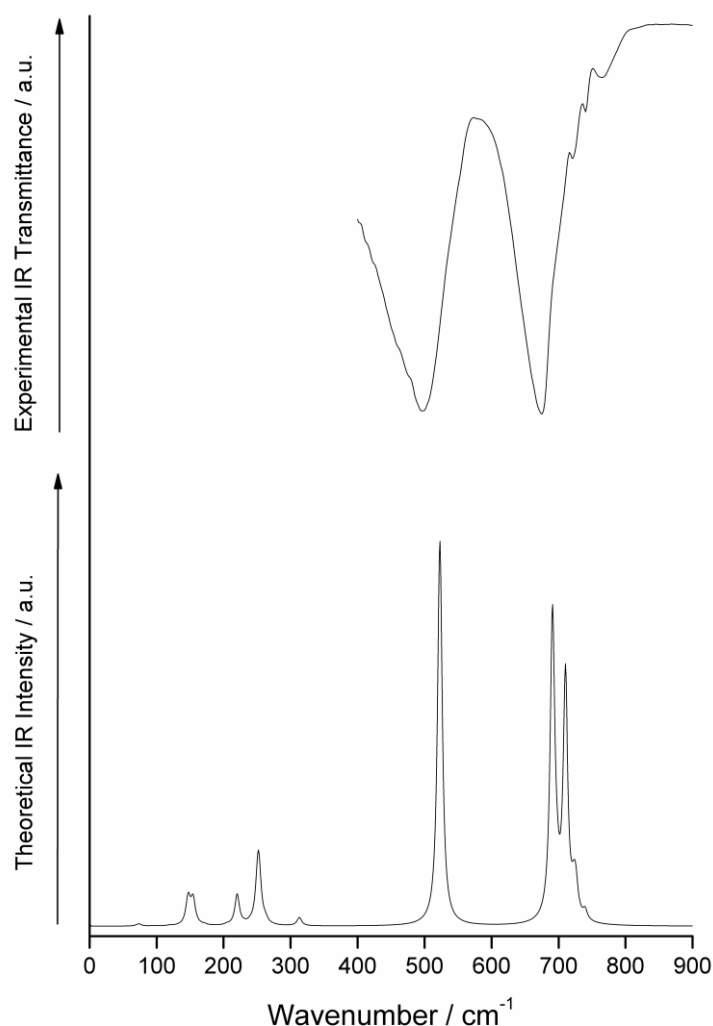


Figure 5. Top: Experimentally obtained IR spectrum of crystalline MoF₅; bottom: Theoretically calculated IR spectrum of the solid state of MoF₅ calculated using the DFT-PBE0 method.

As mentioned earlier, IR spectroscopy of MoF₅ has been previously studied. Acquista and Abramowitz studied differences in the IR spectra of MoF₅ vapors in argon matrices at liquid helium temperatures [9]. These differences occurred by allowing the MoF₅ vapors to reach equilibrium at different temperatures in the range of 25 – 150 °C before being trapped at liquid helium temperatures for measurement. They observed bands at 768, 716, 704 and 231 cm⁻¹ during the room-temperature measurements. At higher temperatures, though, these bands began to decrease in intensity while bands at 713, 683, 261 and 112 cm⁻¹ began to appear. They attributed this observation to the disappearance of polymeric species at higher temperatures and the increase of the monomeric MoF₅ unit. However, a comparison of these IR spectra in argon matrices to the polycrystalline spectrum reported here cannot be made due to the extreme differences in sample handling and measurement techniques. Acquista and Abramowitz also studied a solid-state spectrum of MoF₅ at liquid helium temperatures, which gave rise to broad bands at 725, 700, 660, and 525 cm⁻¹ [9]. Due to its absence in the spectra of heated samples described above, they attributed the band at 525 cm⁻¹ as arising from the fluorine-bridge bond of the tetrameric unit. This band at 525 cm⁻¹ may correspond to the band observed in this work at 496 cm⁻¹, which arises from the symmetric and asymmetric stretching of the Mo – μ-F bonds, in which case the observations of Acquista and Abramowitz may be confirmed. However, the solid-state spectrum of MoF₅ received

from Acquista and Abramowitz [9] is completely different from that reported in this work. This difference, however, may arise from different sample handling techniques and temperature of analysis.

Ouellette and coworkers studied the IR spectrum of a super-cooled liquid of MoF₅ at 25 °C [10]. This spectrum showed bands at approximately 725, 690, 490, 250, 180 and 130 cm⁻¹. Analysis of their liquid MoF₅ data was made on the assumption that monomeric MoF₅ species (of *D*_{3h} symmetry) were present in their melted sample. The liquid IR spectrum obtained from the work of Ouellette and coworkers has similar features when compared to the polycrystalline spectrum obtained in this work, although the peak positions and intensities are different. They also studied the IR spectrum of solid MoF₅ which showed weak bands at 970, 890, 845, 520 and 480 cm⁻¹, medium bands at 200 and 160 cm⁻¹, and very strong bands at 745, 698 and 647 cm⁻¹. The authors did not attempt to make band assignments for the spectrum of solid MoF₅ due to the complexity of the molecule's solid state structure, nor do they state the temperature at which the measurement was performed. Nevertheless, similar features can also be seen in their solid MoF₅ spectrum when compared to the polycrystalline spectrum reported here. The IR bands obtained from this work and previous works can be compared in Table 2.

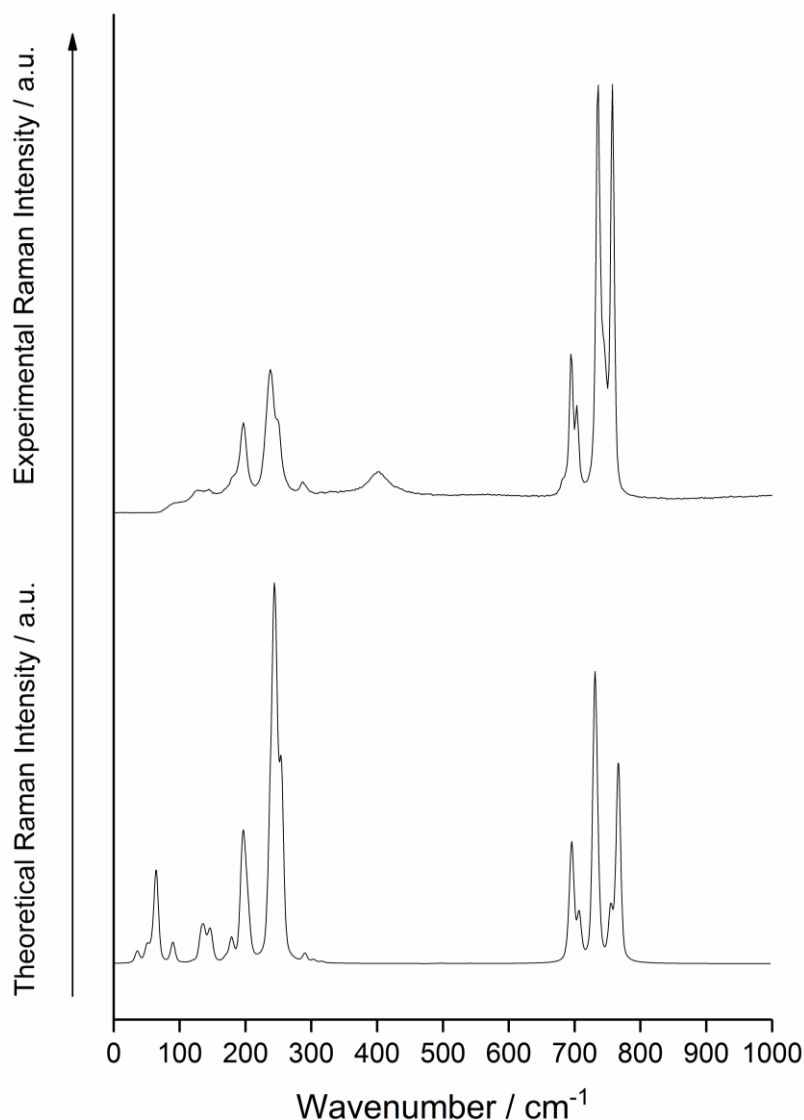
Furthermore, an interesting statement was found in the work of Ouellette and coworkers [10] in which they report the unlikelihood that a reversible change between the tetrameric unit in the solid and a polymeric unit (*n* > 4) in the liquid could be made [10]. This statement was tested in this work through the use of IR spectroscopy to determine if a crystalline sample of MoF₅ decomposes after several melting and cooling cycles to a glassy state characterized by an increased presence of monomers, dimers, or trimers. In this experiment, a sample of MoF₅ was melted at 90 °C and then immediately cooled in liquid nitrogen to produce glassy MoF₅. It was observed that this glassy product quickly reverted back to the crystalline form at room temperature within minutes. Sequential IR spectra taken after nine melting, cooling and annealing (at room temperature) cycles looked identical to the one shown in Figure 5; no new peaks appeared in the range measured. This suggests that any polymeric species present in the melt either recombine or decompose to form the tetramer unit at room temperature. However, our magnetic measurements (see below) showed that cooling rates are of great importance in the conservation of the (MoF₅)_{*n*} species.

Lastly, a Raman spectrum was obtained for a crystalline sample of MoF₅ at room temperature (see Figure 5). This spectrum showed eleven discernible bands at 757, 736, 703, 694, 401, 288, 248, 239, 197, 181 and 134 cm⁻¹. It was compared to a theoretically calculated spectrum obtained for the solid state of MoF₅ using the DFT-PBE0 level of theory. These spectra can be compared in Figure 6. The band locations correlate very well between the experimental and theoretical spectra, however, the band intensities are different. A peak at 401 cm⁻¹ is present in the experimentally obtained Raman spectrum but absent in the theoretically calculated spectrum. This peak may be an overtone of two vibrational modes, or it may arise from a small amount of polymers and/or monomers in the sample, or from an impurity. Band assignments were made using the theoretical Raman spectrum and can be seen in Table 2. Raman spectroscopy of crystalline MoF₅ has previously been studied by Acquista and Abramowitz [9], Ouellette and coworkers [10], and Bates [11]. The spectrum obtained from this work agrees very well with the spectra obtained from these previous studies; they can be compared in Table 2.

1 **Table 2.** Comparison of IR and Raman data obtained in this work and previously reported works [9–11]. Band assignments are given for the IR and Raman spectrum obtained
 2 from this work (ν = vibration; δ = deformation; ρ_r = rocking; ρ_t = twisting). Where two or more band assignments are given, coupling of these optical modes were obtained from
 3 the quantumchemical calculations. Some vibrational assignments are reported without a “symmetrical” or “asymmetrical” classification due to overlap.

| This work IR (crystalline) [cm ⁻¹] | Acquista et al. IR (solid) [cm ⁻¹] | Acquista et al. IR (argon matrix) [cm ⁻¹] | Ouellette et al. IR (solid) [cm ⁻¹] | Ouellette et al. IR (liquid) [cm ⁻¹] | This work Raman (crystalline) [cm ⁻¹] | Acquista et al. Raman (crystalline) [cm ⁻¹] | Ouellette et al. Raman (crystalline) [cm ⁻¹] | Bates Raman (crystalline) [cm ⁻¹] |
|---|--|---|---|--|---|---|--|---|
| | | | 970 | | | | | |
| | | | 890 | | | | | |
| | | | 845 | | | | | |
| 762 $\nu_s(\text{Mo}-\text{F}_{\text{eq}})$ | 725 | 768 | 745 | 725 | 757 $\nu_s(\text{Mo}-\text{F}_{\text{eq}});$ $\nu_{\text{as}}(\text{Mo}-\text{F}_{\text{ax}})$ | 758 | 759 | 759 |
| 739 $\nu(\text{Mo}-\text{F}_{\text{ax}});$ $\nu_{\text{as}}(\text{Mo}-\text{F}_{\text{eq}})^*$ | 700 | 735 | | | | 746 | 746 | 747 |
| 720 $\nu(\text{Mo}-\text{F}_{\text{ax}});$ $\nu(\text{Mo}-\text{F}_{\text{eq}})$ | | 733 | | | 736 $\nu_s(\text{Mo}-\text{F}_{\text{ax}});$ $\nu_s(\text{Mo}-\text{F}_{\text{eq}})$ | 736 | 737 | 738 |
| | | 716 | | | | 704 | 704 | 706 |
| | | 713 | | | 703 $\nu_{\text{as}}(\text{Mo}-\text{F}_{\text{eq}});$ $\nu_{\text{as}}(\text{Mo}-\text{F}_{\text{ax}})$ | | | |
| 675 $\nu_s(\text{Mo}-\text{F}_{\text{terminal}});$ $\nu_{\text{as}}(\text{Mo}-\text{F}_{\text{terminal}})^*$ | 660 | 683 | 698 | 690 | 694 $\nu_{\text{as}}(\text{Mo}-\text{F}_{\text{eq}});$ $\nu_s(\text{Mo}-\text{F}_{\text{terminal}})^*$ | 696 | 696 | 696 |
| | 525 | | 647 | | | 683 | | 684 |
| | | | 520 | | | | 563 | |
| 496 $\nu_s(\text{Mo}-\mu\text{-F});$ $\nu_{\text{as}}(\text{Mo}-\mu\text{-F})^*$ | | | 480 | 490 | 401 | 494 | 406 | 494 |
| | | | | | | 400 | | 436 |
| | | | | | | | | 402 |
| | | | | | | | | 332 |
| | | 261 | 200 | 250 | 288 $\delta(\text{F}_{\text{eq}}-\text{Mo}-\text{F}_{\text{eq}});$ $\delta(\mu\text{-F}-\text{Mo}-\mu\text{-F})$ | 288 | 294 | 282 |
| | | 231 | | | 248 $\delta(\text{F}_{\text{eq}}-\text{Mo}-\text{F}_{\text{eq}})$ 239 $\delta(\text{F}_{\text{eq}}-\text{Mo}-\text{F}_{\text{ax}})$ | 250 | 250 | 252 |
| | | | | | | 236 | 241 | 239 |
| | | 112 | 160 | 180 | 197 $\rho_r(\text{F}_{\text{ax}}-\text{Mo}-\text{F}_{\text{ax}});$ $\rho_t(\text{F}_{\text{eq}}-\text{Mo}-\text{F}_{\text{eq}});$ $\delta(\text{F}_{\text{eq}}-\text{Mo}-\text{F}_{\text{eq}})^*$ | 198 | 198 | 199 |
| | | | | 130 | | 181 | | 181 |
| | | | | | 181 $\delta(\mu\text{-F}-\text{Mo}-\mu\text{-F});$ $\rho_t(\text{F}_{\text{ax}}-\text{Mo}-\text{F}_{\text{ax}})$ | 127 | | |
| | | | | | 134 $\rho_t(\text{F}_{\text{eq}}-\text{Mo}-\text{F}_{\text{eq}});$ $\rho_t(\mu\text{-F}-\text{Mo}-\mu\text{-F});$ $\rho_r(\text{F}_{\text{ax}}-\text{Mo}-\text{F}_{\text{ax}})$ | | | |
| | | | | | | | 59 | |

4 *Indicates two vibrational modes which occur so closely to each other that they could not be resolved into two peaks



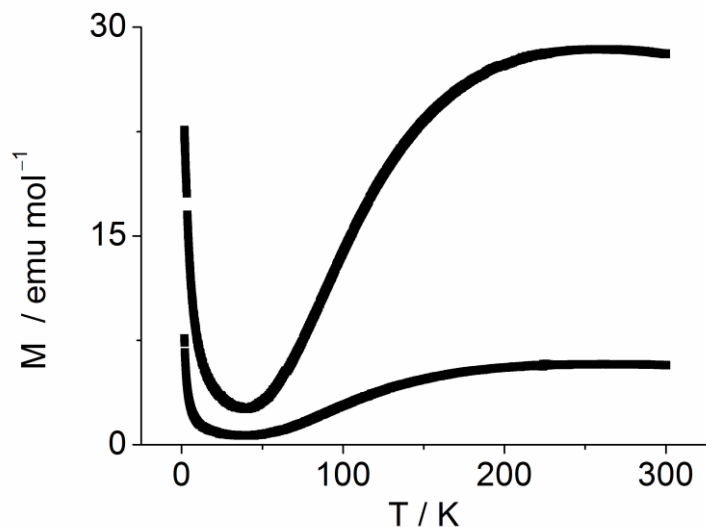
5

6 **Figure 6.** Top: Measured Raman spectrum of crystalline MoF₅; bottom: Theoretical Raman
 7 spectrum of the solid state of MoF₅ calculated using CRYSTAL17 calculations.

8 2.3. Magnetic Measurements

9 Magnetic data of MoF₅ was obtained with the application of the VMS option of a Quantum
 10 Design physical property measurement system (ppms). The material had to be measured in a
 11 homemade FEP sample holder due to the enhanced reactivity of MoF₅ with moisture residues
 12 present in traditional sample holders. The data was corrected with respect to the contribution of the
 13 sample holder as well as the diamagnetic contribution of the sample through utilization of both
 14 experimental data and Pascal constants. The molar diamagnetic susceptibility of MoF₅ was
 15 calculated to be $-6.8 \cdot 10^{-5} \text{ cm}^3 \text{ mol}^{-1}$. Field and temperature dependent magnetic data was also
 16 recorded.

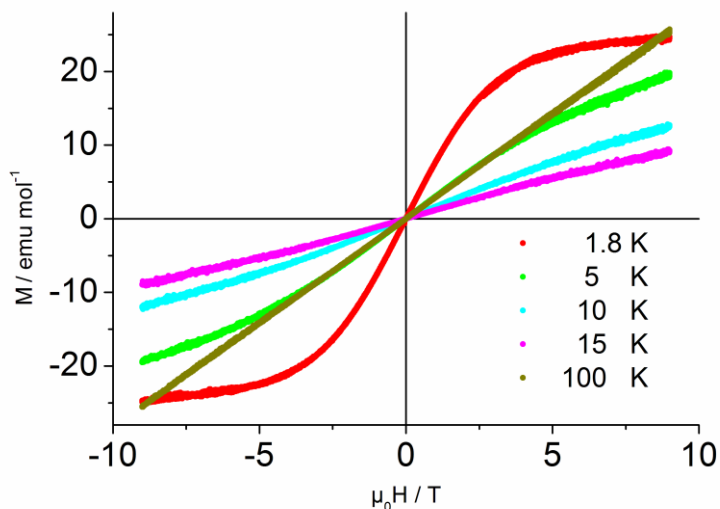
17 Temperature-dependent scans with applied fields of 1 and 5 Tesla were performed in the
 18 temperature range from 1.8 K to 300 K. The curves show a broad maxima at about 260 K. A
 19 decrease in temperature is met with decreasing magnetization, however, at temperatures below 50
 20 K, the magnetization increases once again and reaches values close to the room temperature
 21 measurements (see Figure 7).



22

23 **Figure 7.** Magnetization curve of “MoF₅” at 1 (lower curve) and 5 T (upper curve).

24 Field-dependent measurements of MoF₅ were also carried out at 1.8, 5, 10, 15, 50, 100, 150, 200
 25 and 300 K. Up to 10 K the magnetization data show significantly sigmoidal curves. Above 10 K the
 26 behavior is linear (Figure 8 and Figure S1).



27

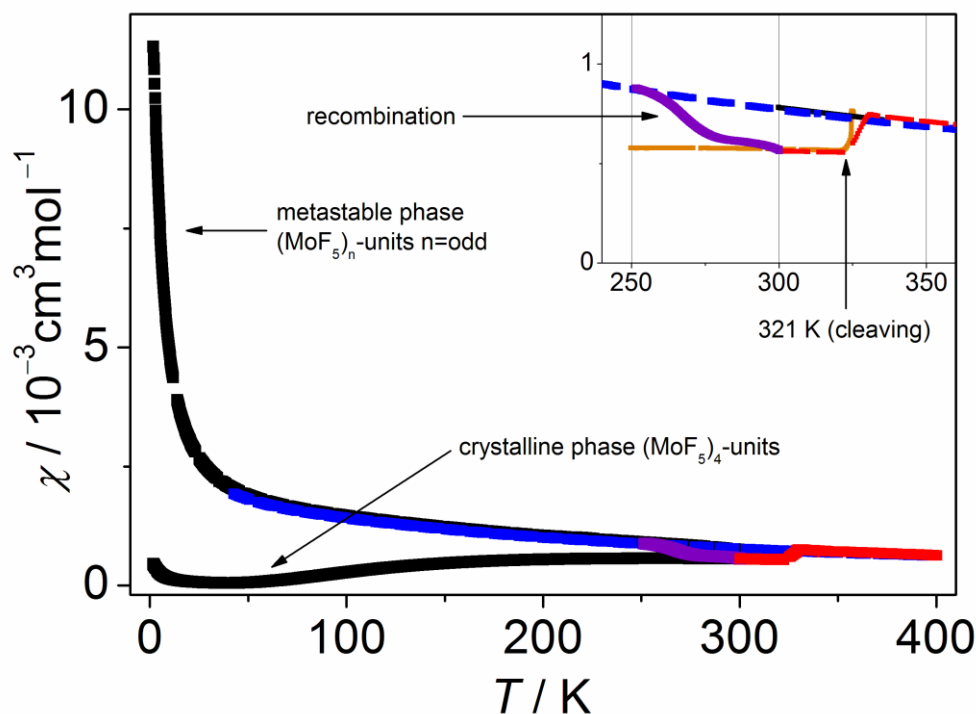
28 **Figure 8.** Field dependent measurements on a crystalline sample of MoF₅.

29 This data describes the magnetic behavior of the crystalline state of MoF₅, which is in good
 30 agreement with the previously reported [14] antiferromagnetism of MoF₅ that is responsible for the
 31 observed maximum at 260 K. The increase of the magnetization below 50 K is an indicator towards
 32 the presence of an additional paramagnetic phase in the sample. This observation indicates the
 33 breakdown of the Mo₄F₂₀ unit into smaller subunits (i.e. monomers, dimers, and trimers). If the
 34 paramagnetic behavior is assumed to stem from species with $S = \frac{1}{2}$, that is, (MoF₅)_n ($n = \text{odd}$)
 35 subunits, their amounts can be estimated to circa 0.3% for $n = 1$, and circa 1% for $n = 3$. These
 36 amounts were determined based on the Brillouin-fit shown in Figure S1. Such amounts are not
 37 observable, or would be very difficult to observe, in a powder X-ray diffraction pattern, so it is
 38 unclear whether the paramagnetic phase is crystalline or amorphous. However, due to the observed

39 ability of MoF₅ to be readily super-cooled [10] and easily transferred to an amorphous state [14], we
40 assume it to also be amorphous in our case.

41 This cooled MoF₅ sample was then warmed above its melting point, leading to an increase in the
42 observed magnetization. The rise in the magnetization curve observed at approximately 321 K is,
43 however, dependent upon the heating rate, as shown in Figure 9. In all cases, though, the content of
44 the paramagnetic species with $S = \frac{1}{2}$ seems to have increased abruptly to approximately 6%
45 (Brillouin-fit in Figure S1), indicating cleavage of the tetramer unit. Upon rapidly cooling the heated
46 sample (20 K/min, indicated by blue curve in Figure 9) a retention of these paramagnetic species
47 seems to occur, as indicated by an observed Curie-Weiss-like magnetic behavior. A Curie-Weiss-fit
48 (Figure S2) yielded a θ value of $-141.7(2)$ K, indicating the presence of somewhat strong
49 antiferromagnetic coupling within this phase. If a Curie-Weiss-fit with two phases, one being a
50 putatively strong antiferromagnetic phase and the other being a paramagnetic phase, is carried out,
51 then the ratio of these two phases can be determined, leading to the calculation of approximately
52 6% paramagnetic, $S = \frac{1}{2}$ species present in the sample.

53 Upon warming of this increased-paramagnetic, metastable phase to 300 K, with a heating rate of
54 2 K/min, a recombination of the (MoF₅)_n species (with $n = \text{odd}$) to (MoF₅)_n (with $n = \text{equal}$; most
55 likely $n = 4$) is likely occurring as indicated by the decrease in susceptibility to the former value of
56 the crystalline phase (as shown by the violet curve in Figure 9). As we cannot observe the sample
57 visually during the magnetic measurements, it remains an open question as to whether the increase
58 in paramagnetic species corresponds to the melting of the compound, or if the tetramers begin to
59 decompose in the solid state. However, melting of the sample is suspected as the temperature
60 nicely corresponds to the reported melting point of high purity MoF₅ [3].



61

62 **Figure 9.** Magnetic susceptibility of two different MoF₅ phases (black). The magnetic behavior
63 during the phase transitions is measured with rising temperatures. The cleavage of the tetramers is
64 shown by the red and orange curves (two separate measurements), the recombination of (MoF₅)_n (n
65 = odd) to (MoF₅)_n ($n = \text{equal}$; very likely $n = 4$) is shown by the violet curve. The rapid cooling of the

66 heated sample with a cooling rate of 20 K/min, which presumably leads to an amorphous state, is
67 shown by the blue curve.

68 2.4 Computational Results

69 Solid MoF₅ (Mo₄F₂₀) was investigated at the DFT-PBE0/TZVP level of theory (see Materials and
70 Methods for full computational details). First, the geometries of two spin configurations were fully
71 optimized, corresponding to the spins of the four Mo atoms in either a ferromagnetic (FM) or
72 antiferromagnetic (AFM) configuration. Both spin configurations could be studied in the original
73 space group *C2/m*. The AFM configuration turned out to be the magnetic ground state, being 5
74 kJ/mol lower in energy in comparison to the ferromagnetic configuration. The absolute value of the
75 spin-only magnetic moment of the Mo atoms is 0.94 μ_B . All solid-state results discussed below have
76 been obtained for the antiferromagnetic ground state.

77 The lattice parameters of the optimized crystal structure are slightly overestimated in
78 comparison to the SCXRD structure (differences in parentheses): $a = 9.74 \text{ \AA}$ (2.8%), $b = 14.39 \text{ \AA}$
79 (1.9%), $c = 5.21 \text{ \AA}$ (2.5%) and $\beta = 95.9^\circ$ (-0.3%). The calculated Mo-F distances showed the same
80 trend as observed in the experimental structure: Mo-F_{bridge} = 2.07 \AA , F_{eq} = 1.84 \AA , and F_{ax} = 1.82 \AA .
81 The IR and Raman spectra calculated for MoF₅ are shown in Figure 5 and Figure 6, respectively. The
82 calculated spectra are in good agreement with the experimental spectrum and enabled the
83 assignment of the vibrational modes.

84 In addition to solid-state MoF₅, the Mo₄F₂₀ molecule was investigated in the gas-phase (DFT-
85 PBE0/def2-TZVP level of theory). The *D*_{2h}-symmetric antiferromagnetic ground state is 7 kJ/mol
86 more stable than the *D*_{4h}-symmetric ferromagnetic spin configuration. We investigated the chemical
87 bonding with the help of Intrinsic Atomic Orbital (IAO) population and Intrinsic Bond Orbitals
88 (IBOs) analysis. The partial atomic charges (e⁻) are as follows: Mo = +2.09, F_{bridge} = -0.55, F_{eq} = -0.40,
89 and F_{ax} = -0.37. The larger the partial charge of an F atom, the longer the calculated Mo-F distance:
90 Mo-F_{bridge} = 2.06 \AA , F_{eq} = 1.82 \AA , and F_{ax} = 1.80 \AA . The longer Mo-F_{eq} distance in comparison to Mo-
91 F_{ax} distance is in agreement with the experimental and computational solid-state results. The
92 elongation of the Mo-F_{eq} can be understood by analyzing the Mo-F bonding in terms of IBOs,
93 which are a physically well-defined form of localized molecular orbitals (MOs) and more suitable
94 for chemical interpretation than the delocalized canonical molecular orbitals. The IBO analysis
95 shown in Figure S3 shows that the highest-energy lone pair orbital of the F_{eq} atom is in complete
96 anti-phase to the Mo $d_{x^2-y^2}$ orbital (unpaired Mo d^1 electron). In the case of the F_{ax} atom, the highest
97 energy lone pair orbital and the Mo $d_{x^2-y^2}$ orbital are not in complete anti-phase and some
98 constructive overlap arises (the IBO has ~10% contribution from Mo). As a consequence, the
99 repulsion between the Mo d^1 electron and the F lone pair electrons is smaller for the F_{ax} atoms than
100 the F_{eq} atoms and the Mo-F_{ax} distance is slightly shorter than the Mo-F_{eq} distance.

101 The energetics of the following (MoF₅)_n species were also studied (molecular geometries are
102 included in the Supporting Information): MoF₅ (C_s); Mo₂F₁₀ (D_{2h}); Mo₃F₁₅ (D_{3h}); Mo₄F₂₀ (D_{4h}); Mo₅F₂₅
103 (D_{5h}). These were gas-phase calculations at 0 K and a ferromagnetic spin configuration was used for
104 all systems since the aim of the study was to understand the structural strain in (MoF₅)_n species and
105 not to investigate the much smaller FM/AFM energy differences. This study gave the relative
106 energies (kJ/mol) per MoF₅ unit, which for n = 1–5 are as follows: 67, 85, 41, 0, and 40. Thus, the
107 concatenation of MoF₅ units is energetically favorable and the Mo₄F₂₀ species is clearly the (MoF₅)_n
108 species with the smallest structural strain.

109 3. Conclusions

110 MoF₅ was synthesized by the reduction of MoF₆ in the presence of CO under UV irradiation. It
111 was confirmed that MoF₅ crystallizes in the monoclinic *C2/m* space group as Mo₄F₂₀ tetramers.
112 Single crystal analysis showed a discernable difference in atomic distance between the Mo-F_{eq} and

113 the Mo—F_{ax} bonds, with the Mo—F_{eq} atomic distances being longer by about 0.02 Å. Theoretical
114 calculations of the Mo₄F₂₀ molecule in the gas-phase (run at the DFT-PBE0/def2-TZVP level of
115 theory) were analyzed using IAO and IBOs. The IBO analysis showed the highest-energy lone pair
116 orbital of the F_{eq} atoms to be in complete anti-phase with the Mo d_{x²-y²} orbital, whereas the highest
117 energy lone pair orbital of the F_{ax} atoms are not in complete anti-phase with the Mo d_{x²-y²} orbital and
118 instead exhibit some constructive overlap. This constructive overlap between orbitals in the Mo—
119 F_{ax} bond is what leads to the slightly shorter bond length of this bond when compared to the Mo—
120 F_{eq} bond.

121 Furthermore, the vibrational spectroscopy study of MoF₅ showed that great differences in the
122 IR spectrum of the molecule can be observed depending on the sample handling and measurement
123 techniques. Polycrystalline IR and Raman spectra are reported here, in which theoretical
124 calculations of solid-state MoF₅ were used to make band assignments. It was shown that of the 69
125 possible optical modes of Mo₄F₂₀, 29 optical modes (18 Raman; 11 IR) could be seen in the
126 computational spectra and 16 (11 Raman; 5 IR) could be seen in the experimental spectra. Band
127 assignments for the experimental spectra can be seen in Table 2.

128 The study of the magnetic properties of a polycrystalline sample of MoF₅ showed the
129 compound to exhibit antiferromagnetic properties, with a maximum observed at 260 K. An increase
130 in magnetism was also observed at temperatures below 50 K. This increase in magnetism is thought
131 to occur from paramagnetic (MoF₅)_n (*n* = odd) subunits with *S* = ½. Warming of the sample lead to
132 an increase of these *S* = ½ subunits, most likely belonging to the monomers and trimers of cleaved
133 Mo₄F₂₀ units. Upon rapid cooling of this sample with increased-paramagnetic behavior, it was
134 shown that this increase in paramagnetism could be preserved. However, upon heating of this
135 increase-paramagnetic, metastable phase back to room temperature, a decrease in magnetism was
136 observed, leading to the conclusion that the paramagnetic, (MoF₅)_n (*n* = odd), species recombined to
137 give the Mo₄F₂₀ tetramers. In support of this conclusion, it was shown through our computational
138 study that the Mo₄F₂₀ unit is the preferred species of “MoF₅”. It seems a fair assessment to conclude
139 from our investigations that, while a small percentage of MoF₅ may be found in the solid state as
140 (MoF₅)_n (*n* = 1-3) units, the preferred species of MoF₅ under ambient conditions is Mo₄F₂₀.

141 4. Materials and Methods

142 4.1. General Procedures and Materials

143 All operations were performed in either stainless steel (316L) or Monel metal Schlenk lines,
144 which were passivated with 100% fluorine at various pressures before use. Preparations were
145 carried out in an atmosphere of dry and purified Argon (5.0, Praxair). Carbon monoxide (5.0, Air
146 Liquide Deutschland) was used as supplied. Molybdenum hexafluoride (99%, ABCR) was distilled
147 once prior to usage. Several UV light bulbs (254 nm, HNS S 11 W G23, Osram Puritec) were used in
148 a homemade chamber to promote MoF₆ reduction.

149 4.2. Synthesis of MoF₅

150 In order to synthesize molybdenum pentafluoride, MoF₆ (3.74 g, 17.80 mmol) was distilled into
151 a 300 mL quartz vessel that was previously evacuated and flamed-dried three times. To this vessel
152 800 mbar (9.69 mmol) of carbon monoxide was added and the reaction vessel was placed into a
153 chamber to allow irradiation by ultraviolet light (254 nm). After 12 hours of irradiation, the product
154 was cooled using liquid nitrogen, the gaseous species in the vessel were evacuated, 800 mbar of
155 fresh carbon monoxide was added, and the vessel was irradiated with UV light for an additional 12
156 hours. After the reaction was complete, all remaining volatile species were evacuated at room
157 temperature and the product (a yellow powder) was transferred into a glovebox for further sample
158 handling. The yield of MoF₅ was quantitative, except for mechanical losses. A powder X-ray

159 diffraction pattern was taken directly from the product with no further sample preparation and
160 confirmed that phase-pure MoF₅ was obtained. The product was found to decompose in air to form
161 a blue hydrolysis product, as expected.

162 In an inert atmosphere, about 200 mg of MoF₅ was transferred to an FEP (fluorinated ethylene
163 propylene) tube and sealed. This tube was placed in an oil bath set to 90 °C in order to melt the
164 sample. Once melted, the MoF₅ was allowed to slowly reach room temperature. This method was
165 used to produce the single crystals used in this study. All other measurements of MoF₅ were
166 performed directly on the powder obtained from the reaction.

167 4.3. Single Crystal X-ray Diffraction

168 X-ray structure analysis of the single crystals of MoF₅ was carried out with a STOE IPDS 2T
169 diffractometer with plane graphite-monochromated molybdenum radiation (Mo-K_α, λ = 0.71073 Å)
170 generated by a sealed X-ray tube (12×0.4 mm long fine focus), and a detector resolution of 6.67
171 pixels mm⁻¹. Evaluation and integration of the diffraction data was carried out using the X-Area
172 software, and an absorption correction was made through integration using the X-Red³² and X-
173 Shape program within the parent software [20]. The structure was solved using the previous
174 structure model of MoF₅ and refined against F² in the SHELXLE software [21,22]. All atoms were
175 located by Difference Fourier synthesis and refined anisotropically. Representations of the crystal
176 structure were created using the Diamond software [23]. Further details of the crystal structure
177 investigation may be obtained from the Fachinformationszentrum Karlsruhe, 76344 Eggenstein-
178 Leopoldshafen, Germany (Fax: +49-7247-808-666; E-Mail: crysdata@fiz-karlsruhe.de,
179 [http://www.fiz-karlsruhe.de/request for deposited data.html](http://www.fiz-karlsruhe.de/request%20for%20deposited%20data.html)) on quoting the depository numbers
180 CSD-433190.

181 4.4. Powder X-ray Diffraction

182 Powder X-ray diffraction patterns were obtained with a Stadi-MP-Diffractometer (STOE) using
183 Cu-K_α radiation (λ = 1.54051 Å), a germanium monochromator, and a Mythen1K detector. The data
184 were handled using the WINXPOW software [24]. The compound was filled into borosilicate
185 capillaries, which were previously flamed dried under vacuum, and sealed using a hot tungsten
186 wire. The powder diffraction pattern presented in this work was obtained using a ring collimator, a
187 step size of 0.195° 2θ, and a measurement time of 125 seconds per step between 0 and 78° 2θ. Using
188 the Jana2006 software [25], a Le Bail refinement was used to fit the powder diffraction pattern. A
189 Chebyshev polynomial employing 15 terms was used for background correction, however, 3 of
190 these 15 terms were omitted from refinement. In order to fit peak shape, a Pseudo-Voigt function
191 was employed. Asymmetry was corrected through divergence.

192 4.5. UV/VIS Spectroscopy

193 The electronic spectrum was measured on a SPECORD 210 PLUS UV/Vis spectrophotometer.
194 The sample was dissolved in perfluoroether and placed into a homemade sample holder with
195 sapphire windows. The spectrum was processed with the WinASPECT Plus software [26].

196 4.6. IR Spectroscopy

197 The IR spectrum was measured on an alpha FTIR spectrometer (Bruker) using a diamond ATR
198 unit under an Ar atmosphere. The spectrum was processed with the OPUS software package [27].

199 4.7. Raman Spectroscopy

200 MoF₅ was loaded into a 0.3 mm borosilicate capillary and the Raman spectrum was measured
201 in backscattering geometry by means of a Raman microscope inVia (Renishaw), using a frequency-

202 doubled Nd:YAG laser (532 nm wavelength). The spectrum was recorded in confocal mode
203 between 2 cm⁻¹ and 1792 cm⁻¹. The laser power was reduced to 5% to prevent degradation of the
204 sample.

205 4.8. Density Determination

206 The density of MoF₅ was measured using the automated gas displacement pycnometry system
207 AccuPyc II 1340 (micromeritics) with a calibrated 0.1 cm³ sample holder and helium as the
208 displacement gas. The number of preliminary purges was set to 30, while the subsequent density
209 measurements were performed 50 times with measurement averaging.

210 4.9. Magnetic Measurements

211 DC-magnetic data were recorded with the VSM option in a Physical Property Measurement
212 System (PPMS Dynacool, Quantum Design, SanDiego, USA). Temperature and field dependent
213 scans were performed in the range from 1.8 to 400 K and from -9 to 9 Tesla. The maximum cooling
214 rate of 20 K/min allows to convert the MoF₅ from its liquid to a super-cooled state.

215 4.10. Computational details

216 Periodic quantum chemical calculations for MoF₅ were carried out using the PBE0 hybrid
217 density functional method (DFT) [28,29]. A polarized triple-zeta-valence (TZVP) level basis set for
218 all atoms was applied. The basis set for molybdenum was derived for this study from the def2-
219 TZVP basis set (details and full basis set listing in Supporting Information) [30]. The basis set for
220 fluorine was taken from our previous study on sodium hydrogen fluorides [31]. All calculations
221 were carried out using the CRYSTAL17 program package [32]. The reciprocal space was sampled
222 using a 5x5x5 Monkhorst-Pack-type *k*-point grid [33]. All calculations were run as spin-unrestricted
223 (the magnetic ground state is described in the main text). For the evaluation of the Coulomb and
224 exchange integrals (TOLINTEG), tight tolerance factors of 8, 8, 8, 8, and 16 were used. Both the
225 atomic positions and lattice constants were fully optimized within the constraints imposed by the
226 space group symmetry. Default optimization convergence thresholds and an extra-large integration
227 grid (XLGRID) were applied in all calculations.

228 The harmonic vibrational frequencies, IR intensities, and Raman intensities were obtained
229 through the use of the computational scheme implemented in CRYSTAL [34–37]. The Raman
230 intensities have been calculated for a polycrystalline powder sample (total isotropic intensity in
231 arbitrary units). The Raman final spectrum was obtained by using pseudo-Voigt peak profile (50:50
232 Lorentzian:Gaussian) and FWHM of 8 cm⁻¹. When simulating the Raman spectrum, the temperature
233 and laser wavelength were set to values corresponding to the experimental setup (T = 298.15 K, λ =
234 532 nm). For the IR spectrum, Lorentzian lineshape and FWHM of 8 cm⁻¹ was used. The peak
235 assignment was carried out by visual inspection of the normal modes (Jmol program package [19]).

236 In addition to the periodic calculations, molecular gas-phase calculations were carried out at
237 the DFT-PBE0/def2-TZVP level of theory using TURBOMOLE program package [30,38,39].
238 Resolution of Identity (RI) approximation was used to speed up the calculations [40,41]. Intrinsic
239 Atomic Orbitals (IAOs) and Intrinsic Bond Orbitals (IBOs) were used in the bonding analysis of the
240 cations [42].

241 Appendix A. Supplementary data

242 Supplementary material related to this article can be found, in the online version, at doi:

243 Acknowledgments

244 Florian Kraus thanks the DFG for funding and Solvay for generous donations of F₂. Antti Karttunen
245 thanks the Academy of Finland for funding (grant 294799) and CSC, the Finnish IT Center for
246 Science, for computational resources. We thank Dr. Klaus Harms of the X-ray facilities at Philipps-
247 Universität Marburg for measurement time, and Dr. Bernhard Roling for allowing us measurement
248 time on his Raman spectrometer. Lastly, we thank Jascha Bandemehr and Lars Deubner for
249 designing an FEP sample holder for the PPMS analysis of MoF₅ and Stefan Rudel for obtaining the
250 single crystal data.

251 **References**

- 252 [1] R.D. Peacock, Proceedings of the Chemical Society. February 1957, Proc. Chem. Soc. (1957) 59.
253 doi:10.1039/ps9570000033.
- 254 [2] J.R. Geichman, E.A. Smith, S.S. Trond, P.R. Ogle, Hexafluorides of Molybdenum, Tungsten, and
255 Uranium. I. Reactions with Nitrous and Nitric Oxides, Inorg. Chem. 1 (1962) 661–665.
256 doi:10.1021/ic50003a042.
- 257 [3] R.F. Krause, T.B. Douglas, The melting temperature, vapor density, and vapor pressure of
258 molybdenum pentafluoride, J. Chem. Thermodyn. 9 (1977) 1149–1163. doi:10.1016/0021-
259 9614(77)90116-1.
- 260 [4] G.H. Cady, G.B. Hargreaves, Vapour pressures of some fluorides and oxyfluorides of
261 molybdenum, tungsten, rhenium, and osmium, J. Chem. Soc. Resumed. (1961) 1568.
262 doi:10.1039/jr9610001568.
- 263 [5] R.T. Paine, L.B. Asprey, Reductive fluoride elimination synthesis of transition metal fluorides.
264 Synthesis of molybdenum pentafluoride and molybdenum tetrafluoride, Inorg. Chem. 13
265 (1974) 1529–1531. doi:10.1021/ic50136a059.
- 266 [6] O.G. Krasnova, G.V. Girichev, A.V. Krasnov, V.D. Butskij, Ehlektronograficheskoe issledovanie
267 stroeniya molekuly MoF₅, Izv. Vysshikh Uchebnykh Zaved. Khimiya Khimicheskaya
268 Tekhnologiya. 37(10–12) (1994) 50–56.
- 269 [7] N.I. Giricheva, O.G. Krasnova, G.V. Girichev, Simultaneous electron diffraction and mass-
270 spectrometric study of the structure of the MoF₅ molecule, J. Struct. Chem. 38 (1997) 54–61.
271 doi:10.1007/BF02768807.
- 272 [8] R.D. Peacock, T.P. Sleight, The electronic spectra of liquid ruthenium and molybdenum
273 pentafluorides, J. Fluor. Chem. 1 (1971) 243–245. doi:10.1016/S0022-1139(00)83218-2.
- 274 [9] N. Acquista, S. Abramowitz, Vibrational spectrum of MoF₅, J. Chem. Phys. 58 (1973) 5484–5488.
275 doi:10.1063/1.1679170.
- 276 [10] T.J. Ouellette, C.T. Ratcliffe, D.W.A. Sharp, Vibrational spectra of molybdenum and tungsten
277 pentafluorides, J. Chem. Soc. Inorg. Phys. Theor. (1969) 2351. doi:10.1039/j19690002351.
- 278 [11] J.B. Bates, Raman spectrum of crystalline MoF₅, Spectrochim. Acta Part Mol. Spectrosc. 27
279 (1971) 1255–1258. doi:10.1016/0584-8539(71)80077-6.
- 280 [12] Y.V. Vasil'ev, A.A. Opalovskii, K.A. Khaldoyanidi, Magnetic properties of molybdenum
281 pentafluoride, Bull. Acad. Sci. USSR Div. Chem. Sci. 18 (1969) 231–233. doi:10.1007/BF00905525.
- 282 [13] A.M. Panich, V.K. Goncharuk, S.P. Gabuda, N.K. Moroz, Molecular and electronic structure of
283 molybdenum pentafluoride, J. Struct. Chem. 20 (1979) 45–47. doi:10.1007/BF00746290.
- 284 [14] V.N. Ikorskii, K.A. Khaldoyanidi, Structural and phase transformations of molybdenum
285 pentafluoride, J. Struct. Chem. 23 (1982) 302–304. doi:10.1007/BF00790778.
- 286 [15] A.J. Edwards, R.D. Peacock, R.W.H. Small, The preparation and structure of molybdenum
287 pentafluoride, J. Chem. Soc. Resumed. (1962) 4486. doi:10.1039/jr9620004486.
- 288 [16] A.J. Edwards, G.R. Jones, Fluoride crystal structures. Part I. Tungsten oxide tetrafluoride, J.
289 Chem. Soc. Inorg. Phys. Theor. (1968) 2074. doi:10.1039/j19680002074.
- 290 [17] B.J. Coe, S.J. Glenwright, Trans-effects in octahedral transition metal complexes, Coord. Chem.
291 Rev. 203 (2000) 5–80. doi:10.1016/S0010-8545(99)00184-8.

- 292 [18] E.M. Shustorovich, M.A. Porai-Koshits, Y.A. Buslaev, The mutual influence of ligands in
293 transition metal coordination compounds with multiple metal-ligand bonds, *Coord. Chem.*
294 *Rev.* 17 (1975) 1–98. doi:10.1016/S0010-8545(00)80300-8.
- 295 [19] Jmol: an open-source Java viewer for chemical structures in 3D. <http://www.jmol.org/>, n.d.
- 296 [20] X-Area, STOE & Cie GmbH, Darmstadt, Germany, 2011.
297 <https://www.stoe.com/product/software-x-area/>.
- 298 [21] G.M. Sheldrick, A short history of *SHELX*, *Acta Crystallogr. A.* 64 (2008) 112–122.
299 doi:10.1107/S0108767307043930.
- 300 [22] G.M. Sheldrick, Crystal structure refinement with *SHELXL*, *Acta Crystallogr. Sect. C Struct.*
301 *Chem.* 71 (2015) 3–8. doi:10.1107/S2053229614024218.
- 302 [23] H. Putz, K. Brandenburg, *Diamond - Crystal and Molecular Structure Visualization*, Crystal
303 Impact, Bonn, Germany, 2015. <http://www.crystalimpact.com/diamond>.
- 304 [24] STOE WinXPOW, STOE & Cie GmbH, Darmstadt, Germany, 2011.
- 305 [25] V. Petříček, M. Dušek, L. Palatinus, Crystallographic Computing System JANA2006: General
306 features, *Z. Für Krist. - Cryst. Mater.* 229 (2014). doi:10.1515/zkri-2014-1737.
- 307 [26] WinASPECT Plus, Jena, Germany, 2014.
- 308 [27] OPUS, Bruker Optik GmbH, Ettlingen, Germany, 2009.
- 309 [28] J.P. Perdew, K. Burke, M. Ernzerhof, Generalized Gradient Approximation Made Simple, *Phys.*
310 *Rev. Lett.* 77 (1996) 3865–3868. doi:10.1103/PhysRevLett.77.3865.
- 311 [29] C. Adamo, V. Barone, Toward reliable density functional methods without adjustable
312 parameters: The PBE0 model, *J. Chem. Phys.* 110 (1999) 6158–6170. doi:10.1063/1.478522.
- 313 [30] F. Weigend, R. Ahlrichs, Balanced basis sets of split valence, triple zeta valence and quadruple
314 zeta valence quality for H to Rn: Design and assessment of accuracy, *Phys. Chem. Chem. Phys.*
315 7 (2005) 3297. doi:10.1039/b508541a.
- 316 [31] S.I. Ivlev, T. Soltner, A.J. Karttunen, M.J. Mühlbauer, A.J. Kornath, F. Kraus, Syntheses and
317 Crystal Structures of Sodium Hydrogen Fluorides NaF· *n* HF (*n* = 2, 3, 4): Syntheses and Crystal
318 Structures of Sodium Hydrogen Fluorides NaF· *n* HF (*n* = 2, 3, 4), *Z. Für Anorg. Allg. Chem.*
319 643 (2017) 1436–1443. doi:10.1002/zaac.201700228.
- 320 [32] R. Dovesi, A. Erba, R. Orlando, C.M. Zicovich-Wilson, B. Civalleri, L. Maschio, M. Rérat, S.
321 Casassa, J. Baima, S. Salustro, B. Kirtman, Quantum-mechanical condensed matter simulations
322 with CRYSTAL, *Wiley Interdiscip. Rev. Comput. Mol. Sci.* (2018) e1360. doi:10.1002/wcms.1360.
- 323 [33] H.J. Monkhorst, J.D. Pack, Special points for Brillouin-zone integrations, *Phys. Rev. B.* 13 (1976)
324 5188–5192. doi:10.1103/PhysRevB.13.5188.
- 325 [34] F. Pascale, C.M. Zicovich-Wilson, F. López Gejo, B. Civalleri, R. Orlando, R. Dovesi, The
326 calculation of the vibrational frequencies of crystalline compounds and its implementation in
327 the CRYSTAL code, *J. Comput. Chem.* 25 (2004) 888–897. doi:10.1002/jcc.20019.
- 328 [35] C.M. Zicovich-Wilson, F. Pascale, C. Roetti, V.R. Saunders, R. Orlando, R. Dovesi, Calculation
329 of the vibration frequencies of alpha-quartz: The effect of Hamiltonian and basis set, *J. Comput.*
330 *Chem.* 25 (2004) 1873–1881. doi:10.1002/jcc.20120.
- 331 [36] L. Maschio, B. Kirtman, M. Rérat, R. Orlando, R. Dovesi, *Ab initio* analytical Raman intensities
332 for periodic systems through a coupled perturbed Hartree-Fock/Kohn-Sham method in an
333 atomic orbital basis. I. Theory, *J. Chem. Phys.* 139 (2013) 164101. doi:10.1063/1.4824442.
- 334 [37] L. Maschio, B. Kirtman, M. Rérat, R. Orlando, R. Dovesi, *Ab initio* analytical Raman intensities
335 for periodic systems through a coupled perturbed Hartree-Fock/Kohn-Sham method in an

336 atomic orbital basis. II. Validation and comparison with experiments, *J. Chem. Phys.* 139 (2013)
337 164102. doi:10.1063/1.4824443.

338 [38] TURBOMOLE V7.2 2017, a development of University of Karlsruhe and Forschungszentrum
339 Karlsruhe GmbH, 1989-2007, TURBOMOLE GmbH, since 2007; available from
340 <http://www.turbomole.com>, n.d.

341 [39] R. Ahlrichs, M. Bär, M. Häser, H. Horn, C. Kölmel, Electronic structure calculations on
342 workstation computers: The program system turbomole, *Chem. Phys. Lett.* 162 (1989) 165–169.
343 doi:10.1016/0009-2614(89)85118-8.

344 [40] K. Eichkorn, O. Treutler, H. Öhm, M. Häser, R. Ahlrichs, Auxiliary basis sets to approximate
345 Coulomb potentials, *Chem. Phys. Lett.* 240 (1995) 283–290. doi:10.1016/0009-2614(95)00621-A.

346 [41] F. Weigend, Accurate Coulomb-fitting basis sets for H to Rn, *Phys. Chem. Chem. Phys.* 8 (2006)
347 1057. doi:10.1039/b515623h.

348 [42] G. Knizia, Intrinsic Atomic Orbitals: An Unbiased Bridge between Quantum Theory and
349 Chemical Concepts, *J. Chem. Theory Comput.* 9 (2013) 4834–4843. doi:10.1021/ct400687b.
350